Journal of Computational Mathematics
Vol.31, No.4, 2013, 355–369.

http://www.global-sci.org/jcm
doi:10.4208/jcm.1301-m4021

EVALUATION OF SINGULAR AND NEARLY SINGULAR INTEGRALS IN THE BEM WITH EXACT GEOMETRICAL REPRESENTATION*

Yaoming Zhang
Institute of Applied Mathematics, Shandong University of Technology, Zibo 255049, China
State Key Laboratory of Structural Analysis for Industrial Equipment, Dalian University of Technology, Dalian 116024, China
Email: zymfc@163.com
Wenzhen Qu Yan Gu
Center for Numerical Simulation software in Engineering and Sciences, Department of Engineering Mechanics, Hohai University, Nanjing 210098, China
Email: qwzxxoo7@163.com guyan1973@163.com

Abstract

The geometries of many problems of practical interest are created from circular or elliptic arcs. Arc boundary elements can represent these boundaries exactly, and consequently, errors caused by representing such geometries using polynomial shape functions can be removed. To fully utilize the geometry of circular boundary, the non-singular boundary integral equations (BIEs) and a general nonlinear transformation technique available for arc elements are introduced to remove or damp out the singular or nearly singular properties of the integral kernels. Several benchmark 2D elastostatic problems demonstrate that the present algorithm can effectively handle singular and nearly singular integrals occurring in the boundary element method (BEM) for boundary layer effect and thin-walled structural problems. Owing to the employment of exact geometrical representation, only a small number of elements need to be divided along the boundary and high accuracy can be achieved without increasing other more computational efforts.

Mathematics subject classification: 68Q05.
Key words: BEM, Singular integrals, Nearly singular integrals, Boundary layer effect, Thin walled structures, Exact geometrical representation.

1. Introduction

The BEM is a powerful and efficient computational method if boundary integrals can be evaluated accurately. The main advantage of the BEM resulting from the reduction of the dimension of the boundary value problem is well-known. However, it is popular as well that the standard BEM formulations include singular and nearly singular integrals, and thus the integrations should be performed very carefully. In the past decades, many direct and indirect algorithms for singular integral have been developed and used successfully [1-11]. The nearly singular integrals, however, need to be further studied, although great progresses have been achieved for each of the existing methods. Studies show that the conventional boundary element method (CBEM) using the standard Gaussian quadrature fails to yield reliable results for nearly singular integrals. The major reason for this failure is that the kernels' integration

* Received January 15, 2012 / Revised version received January 21, 2013 / Accepted January 31, 2013 / Published online July 9, 2013 /

presents various orders of near singularities since the integrand oscillates very fiercely within the integration interval. Therefore, although nearly singular integrals are not singular in the sense of mathematics, it can not be calculated accurately by the standard Gaussian quadrature.

Nearly singular integrals usually occur for the thin-body problem when the thickness of the considered domain is small, or for the case where the physical quantity is calculated at a domain point which is very close to the boundary, or for the case where the mesh contains a large element and a small element adjacent to each other. The usual approach to achieving high accuracy is to use the subdivision method which is done to increase the number of subdivisions as the source point gets close to the element where the integral is taken. However, this method requires too much preprocessing and CPU time, especially for solving thin-body problems.

In the past decades, tremendous effort was devoted to derive convenient integral forms or sophisticated computational techniques for calculating the nearly singular integrals. These proposed methods can be divided on the whole into two categories: "indirect algorithms" and "irect algorithms". The indirect algorithms [4,9-11], which benefit from the regularization ideas and techniques for the singular integrals, are mainly to calculate indirectly or avoid calculating the nearly singular integrals by establishing new regularized boundary integral equations (BIEs). However, the accuracy of their calculated results is not very satisfactory. The direct algorithms are calculating the nearly singular integrals directly. They usually include, but are not limited to, interval subdivision method [12-13], special Gaussian quadrature method [14-15], the exact integration method [16-18], and nonlinear transformation method [19-23]. Although great progresses have been achieved for each of the above methods, it should be pointed out that the geometry of the boundary element is often depicted by using linear shape functions when nearly singular integrals need to be calculated [22]. However, most engineering processes occur mostly in complex geometrical domains, and obviously, higher order geometry elements are expected to be more accurate to solve such practical problems [1-4]. Recently, two regularized algorithms suitable for calculating the nearly singular integrals occurring on the high-order geometry elements was proposed by the authors of this paper [18,23].

It is well known that the accuracy is a vital factor in a successful calculation, together with minimum computer storage and CPU time. There are several sources of inaccuracy in the boundary element method. They are the use of polynomial shape functions to represent the boundary geometries, also to represent the variations of the physical variables over the boundary, the numerical integrations using Gaussian quadrature, and the rounding off errors during the evaluations.

The geometries of many problems of practical interest are created from circular or elliptic arcs. Arc boundary elements can represent circular and elliptic boundaries exactly, and consequently, errors caused by representing such geometries using polynomial shape functions can be removed by using exact geometrical representations. Therefore, the exact geometrical representation is expected to give more accurate results than lower-order or even high-order boundary element analysis.

To fully utilize the geometry of circular boundary, the approach used in this paper is exact geometrical representation for circular and elliptic boundaries. Both singular and nearly singular integrals are reconstructed and calculated under such geometrical representation. To verify the method developed in this paper, both boundary layer effect and thin body problems are considered. For boundary layer effect, the stresses at the interior points very close to boundary are evaluated. For thin body problems, very promising results are obtained when the thickness-to-length ratios is in the orders from 10^{-1} to 10^{-9}, which is sufficient for mod-

eling most thin-walled structures in the micro- or nano- scales. Owing to the employment of exact geometrical representation, only a small number of elements need to be divided along the boundary and high accuracy can be achieved without increasing other more computational efforts.

2. Non-Singular BIEs for 2D Elastic Problems

It is well known that the domain variables can be computed by integral equations only after all the boundary quantities have been obtained, and the accuracy of boundary quantities directly affects the validity of the interior quantities. However, when calculating the boundary quantities, we have to deal with the singular boundary integrals, and a good choice is using the regularized Boundary Integral Equations(BIEs). In this paper, we always assume that is a bounded domain in , is its open complement, and denotes the boundary. and (or and) are the unit tangent and outward normal vectors of to the domain at the point , respectively. For 2-D elastic problems, the non-singular BIEs with indirect variables can be found in [5]. Without regard to the rigid body displacement and the body forces, the regularized BIEs excluding the CPV and HFP integrals, on can be expressed as

$$u_i(\boldsymbol{y}) = \int_\Gamma \phi_k(\boldsymbol{x}) u^*_{ik}(\boldsymbol{y},\boldsymbol{x}) d\Gamma, \quad \boldsymbol{y} \in \Gamma, \tag{2.1}$$

$$\begin{aligned}\nabla u_i(\boldsymbol{y}) = &\int_\Gamma [\phi_k(\boldsymbol{x}) - \phi_k(\boldsymbol{y})] \nabla u^*_{ik}(\boldsymbol{y},\boldsymbol{x}) d\Gamma - \phi_k(\boldsymbol{y}) \left\{ \int_\Gamma [\boldsymbol{t}(\boldsymbol{x}) - \boldsymbol{t}(\boldsymbol{y})] \frac{\partial u^*_{ik}(\boldsymbol{y},\boldsymbol{x})}{\partial \boldsymbol{t}} d\Gamma \right. \\ &+ \int_\Gamma [\boldsymbol{n}(\boldsymbol{x}) - \boldsymbol{n}(\boldsymbol{y})] \frac{\partial u^*_{ik}(\boldsymbol{y},\boldsymbol{x})}{\partial \boldsymbol{n}} d\Gamma + \frac{k_0}{G} \boldsymbol{n}(\boldsymbol{y}) \left(\int_\Gamma [n_k(\boldsymbol{x}) - n_k(\boldsymbol{y})] \frac{\partial \ln r}{\partial x_i} d\Gamma \right. \\ &\left. \left. + n_k(\boldsymbol{y}) \int_\Gamma [t_i(\boldsymbol{x}) - t_i(\boldsymbol{y})] \frac{\partial \ln r}{\partial \boldsymbol{t}} d\Gamma n_k(\boldsymbol{y}) \int_\Gamma [n_i(\boldsymbol{x}) - n_i(\boldsymbol{y})] \frac{\partial \ln r}{\partial \boldsymbol{n}} d\Gamma \right) \right\}, \quad \boldsymbol{y} \in \Gamma,\end{aligned} \tag{2.2}$$

where $i, k = 1, 2$; $k_0 = 1/4\pi(1-v)$; G is the shear modulus; $\phi_k(x)$ is the density function to be determined; r is the distance between load point and field point.

For the domain Ω, the regularized BIEs excluding the CPV and HFP integrals, are given as

$$u_i(\boldsymbol{y}) = \int_\Gamma \phi_k(\boldsymbol{x}) u^*_{ik}(\boldsymbol{x},\boldsymbol{y}) d\Gamma, \quad \boldsymbol{y} \in \Gamma, \tag{2.3}$$

$$\begin{aligned}\nabla u_i(\mathbf{y}) = &\phi_k(\boldsymbol{y}) \boldsymbol{n}(\boldsymbol{y}) \frac{1}{G} [\delta_{ik} - \frac{n_k(\boldsymbol{y}) n_i(\boldsymbol{y})}{2(1-v)}] + \int_\Gamma [\phi_k(\boldsymbol{x}) - \phi_k(\boldsymbol{y})] \nabla u^*_{ik}(\boldsymbol{y},\boldsymbol{x}) d\Gamma \\ &- \phi_k(\boldsymbol{y}) \left\{ \int_\Gamma [\boldsymbol{t}(\boldsymbol{x}) - \boldsymbol{t}(\boldsymbol{y})] \frac{\partial u^*_{ik}(\boldsymbol{y},\boldsymbol{x})}{\partial \boldsymbol{t}} d\Gamma + \int_\Gamma [\boldsymbol{n}(\boldsymbol{x}) - \boldsymbol{n}(\boldsymbol{y})] \frac{\partial u^*_{ik}(\boldsymbol{y},\boldsymbol{x})}{\partial \boldsymbol{n}} d\Gamma \right. \\ &+ \frac{k_0}{G} \boldsymbol{n}(\boldsymbol{y}) \left(\int_\Gamma [n_k(\boldsymbol{x}) - n_k(\boldsymbol{y})] \frac{\partial \ln r}{\partial x_i} d\Gamma + n_k(\boldsymbol{y}) \int_\Gamma [t_i(\boldsymbol{x}) - t_i(\boldsymbol{y})] \frac{\partial \ln r}{\partial \boldsymbol{t}} d\Gamma \right. \\ &\left. \left. + n_k(\boldsymbol{y}) \int_\Gamma [n_i(\boldsymbol{x}) - n_i(\boldsymbol{y})] \frac{\partial \ln r}{\partial \boldsymbol{n}} d\Gamma \right) \right\}, \quad \boldsymbol{y} \in \Gamma.\end{aligned} \tag{2.4}$$

For the internal point y, the integral equations can be written as

$$u_i(\boldsymbol{y}) = \int_\Gamma \phi_k(\boldsymbol{x}) u^*_{ik}(\boldsymbol{y},\boldsymbol{x}) d\Gamma, \qquad \boldsymbol{y} \in \hat{\Omega}, \tag{2.5}$$

$$\nabla u_i(\boldsymbol{y}) = \int_\Gamma \phi_k(\boldsymbol{x}) \nabla u^*_{ik}(\boldsymbol{y},\boldsymbol{x}) d\Gamma, \quad \boldsymbol{y} \in \hat{\Omega}, \tag{2.6}$$

where $\hat{\Omega} = \Omega$ or Ω^c.

In Eqs. (2.1) - (2.6), $u^*_{ik}(\boldsymbol{y}, \boldsymbol{x})$ denotes the Kelvin displacement fundamental solution and can be expressed as

$$u^*_{ik}(\boldsymbol{y}, \boldsymbol{x}) = \frac{1}{8\pi G(1-\mu)} \left[(3-4\mu)\delta_{ik} \ln \frac{1}{r} + \frac{\partial r}{\partial x_i} \frac{\partial r}{\partial x_k} \right]. \tag{2.7}$$

3. Numerical Implementation

3.1. Exact geometrical representation

The quintessence of the BEM is to discretize the boundary into a finite number of segments, not necessarily equal, which are called boundary elements. Two approximations are made over each of these elements. One is about the geometry of the boundary, while the other has to do with the variation of the unknown boundary quantity over the element. The linear element is not an ideal one as it can not approximate with sufficient accuracy for the geometry of curvilinear boundaries. For this reason, it is recommended to use higher order elements, and most often, using isoparametric quadratic elements in most applications. Since a substantial proportion of domains of interest in practice are created from circular or elliptic arcs, exact geometrical representations for such geometries can greatly improve the accuracies of the numerical analyses. However, for thin body structural problems, the advantage of using exact geometrical representation is not only concerning its power to improve the calculation accuracy. More importantly, computational models of these structures demand a higher level of the geometry approximation, and the usage of exact geometrical representation in computational models can meet this requirement. For example, if the boundary geometry is depicted by using the straight line, the linear element of the outer surface will attach or even pass through the inner boundary if the thickness of the considered structure is very small, as shown in Fig. 3.1. Consequently, the actual geometry of considered domain can not be described lively, and thus lower-order geometry approximation will fail to yield reliable results for such problems. In order to avoid this phenomenon, very fine meshes mush be used in this situation, but this yields too much preprocessing and CPU time.

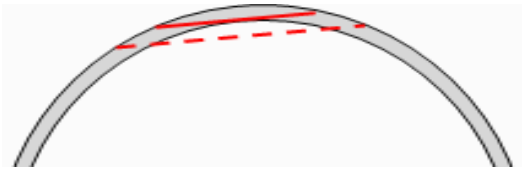

Fig. 3.1. A thin-walled structure with illogical geometry element.

The exact geometrical representation, namely "arc element", for circular and elliptic boundaries has been proposed by Zhang [5]. Consider a circular arc element of radius of curvature R with its centre of curvature located at (x'_1, x'_2) as in Fig. 3.2. Suppose $(R,\ \theta_1), (R,\ \theta_2)$, are the coordinates of the two extreme points of the arc element Γ_j, respectively.

The exact boundary elements can be expressed as

$$\begin{cases} x_1 = x'_1 + R\cos\theta_\xi, \\ x_2 = x'_2 + R\sin\theta_\xi, \end{cases} \tag{3.1}$$

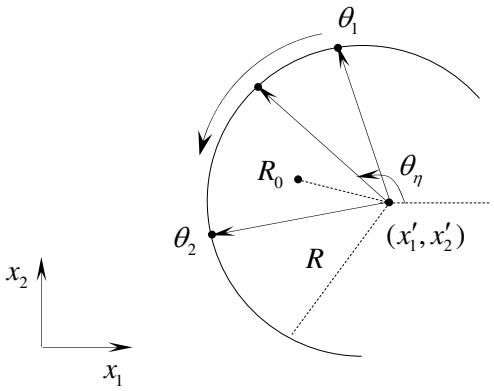

Fig. 3.2. An element on a circular boundary segment.

where $\theta_\xi = \frac{1-\xi}{2}\theta_1 + \frac{1+\xi}{2}\theta_2,\ (-1 \le \xi \le 1)$.

The Jacobian of transformation from arc element to intrinsic coordinate ξ reduces to

$$J(\xi) = \frac{1}{2}\sqrt{(x_1^2 - x_1^1)^2 + (x_2^2 - x_2^1)^2} = R\frac{\theta_2 - \theta_1}{2}. \tag{3.2}$$

When the collocation point $\boldsymbol{y}$ locates on the boundary Γ, its coordinates can be expressed as (for simplicity, suppose $(x_1', x_2') = (0, 0)$)

$$y_1 = R\cos\theta_\eta, \quad y_2 = R\sin\theta_\eta, \tag{3.3}$$

where $\theta_\eta = \frac{1-\eta}{2}\theta_1 + \frac{1+\eta}{2}\theta_2, \eta \in (-1, 1)$ is the local coordinate of the point $\boldsymbol{y}$.

3.2. Numerical Implementation for singular integrals

In boundary element analysis, the discretized boundary integrals would present various orders of singularity when the source point and the field point coincide and the distance r equals zero. An effective technique to handle these singular integrals is critical to achieve efficient, accurate boundary element analysis. In section 2, an effective non-singular boundary integral equations for 2D elastic problems is introduced, herein we will discuss its numerical implementations on arc elements.

If the boundary of the solution domain is divided into a total of N elements, Eqs. (2.1) and (2.3) become

$$u_i(\boldsymbol{y}) = \sum_{m=1}^{N}\sum_{s=1}^{3}\phi_k(\boldsymbol{x}_{(m,c)})\int_{-1}^{1} J(\xi)N_s(\xi)u_{ik}^*(\boldsymbol{y}, \boldsymbol{x})d\xi, \tag{3.4}$$

where $J(\xi) = R\frac{\theta_2-\theta_1}{2}, N_1(\xi) = \frac{1}{2}\xi(\xi-1), N_2(\xi) = 1-\xi^2, N_3(\xi) = \frac{1}{2}\xi(\xi+1)$.

When the load point does not lie on the element over which the integration is being performed, the standard Gaussian quadrature technique can be used to evaluate the integrals. However, when the load point does lie on the element, special treatments of the integrals are needed. The right hand of Eq. (3.4) can be expressed as follows

$$\begin{aligned}&\int_{-1}^{1} J(\xi)N_s(\xi)u_{ik}^*(\boldsymbol{y}, \boldsymbol{x})d\xi \\ &= \frac{1}{8\pi G(1-\mu)}\left\{(3-4\mu)\delta_{ik}\int_{-1}^{1} J(\xi)N_s(\xi)\ln\frac{1}{r}d\xi + \int_{-1}^{1} J(\xi)N_s(\xi)\frac{\partial r}{\partial x_i}\frac{\partial r}{\partial x_k}d\xi\right\}.\end{aligned} \tag{3.5}$$

Obviously, there is no singularity in the second right hand side integral, it therefore can be evaluated using standard Gaussian quadrature. The first hand side integral, however, requires special treatment because of the singularity when the load point lies on the element. There are several methods available to evaluate this kind of integral in boundary element implementations, most of which fall into the categories of either coordinate transformation or interval splitting. When the load point is the first node of the element, $r = 2R\sin[(1+\xi)(\theta_2-\theta_1)/4]$, the first right hand side integral of Eq. (3.5) becomes

$$\begin{aligned} I &= -\int_{-1}^{1} J(\xi)N_s(\xi)\ln\left[2R\sin\frac{(1+\xi)(\theta_2-\theta_1)}{4}\right]d\xi \\ &= \int_{-1}^{1} J(\xi)N_s(\xi)\ln\left[\frac{(1+\xi)/2}{2R\sin\frac{(1+\xi)(\theta_2-\theta_1)}{4}}\right]d\xi + \int_{-1}^{1} J(\xi)N_s(\xi)\ln\frac{2}{1+\xi}d\xi. \end{aligned} \tag{3.6}$$

The first right hand side integral can now be evaluated by using standard Gaussian quadrature. Transformed second integral via $\xi = 2\eta - 1$, then this part can be evaluated using logarithmic schemes.

Similar treatment is needed for the case where the load point is the middle or third node of the element [24].

When considering the Eqs. (2.2) and (2.4), the unit tangent and outward normal vectors of Γ to the domain Ω can be expressed as follows

$$t_1(\boldsymbol{x}) = \frac{1}{J(\xi)}\frac{dx_1}{d\xi} = -\sin(\theta_\xi),\quad t_2(\boldsymbol{x}) = \frac{1}{J(\xi)}\frac{dx_2}{d\xi} = \cos(\theta_\xi), \tag{3.7a}$$

$$t_1(\boldsymbol{y}) = \frac{1}{J(\eta)}\left.\frac{dy_1}{d\xi}\right|_{\xi=\eta} = -\sin(\theta_\eta),\quad t_2(\boldsymbol{y}) = \frac{1}{J(\eta)}\left.\frac{dy_2}{d\xi}\right|_{\xi=\eta} = \cos(\theta_\eta), \tag{3.7b}$$

$$n_1(\boldsymbol{x}) = \frac{1}{J(\xi)}\frac{dx_2}{d\xi} = \cos(\theta_\xi),\quad n_2(\boldsymbol{x}) = -\frac{1}{J(\xi)}\frac{dx_1}{d\xi} = \sin(\theta_\xi), \tag{3.8a}$$

$$n_1(\boldsymbol{y}) = \frac{1}{J(\eta)}\left.\frac{dy_2}{d\xi}\right|_{\xi=\eta} = \cos(\theta_\eta),\quad n_2(\boldsymbol{y}) = -\frac{1}{J(\eta)}\left.\frac{dy_1}{d\xi}\right|_{\xi=\eta} = \sin(\theta_\eta). \tag{3.8b}$$

The integral kernels of the discretized equations (2.2) and (2.4) contain the following forms

$$\begin{cases} \dfrac{\partial u^*_{ik}(\boldsymbol{x},\boldsymbol{y})}{\partial \boldsymbol{t}} = \sin^{-1}\left[(\theta_2-\theta_1)\dfrac{(\eta-\xi)}{4}\right] f_{ik}, \\ \dfrac{\partial u^*_{ik}(\boldsymbol{x},\boldsymbol{y})}{\partial \boldsymbol{n}} = \sin^{-1}\left[(\theta_2-\theta_1)\dfrac{(\eta-\xi)}{4}\right] g_{ik}, \end{cases} \quad (i,k=1,2), \tag{3.9}$$

where f_{ik} and g_{ik} are regular functions which will not present (near)singularities. Clearly, the above functions would present singularity when $\xi \to \eta$.

If $\phi(\boldsymbol{x}), \boldsymbol{n}(\boldsymbol{x})$ and $\boldsymbol{t}(\boldsymbol{x})$ satisfies the Hölder condition, viz. $\phi(\boldsymbol{x}) \in C^{0,\alpha_1}, \boldsymbol{n}(\boldsymbol{x}) \in C^{0,\alpha_2}, \boldsymbol{t}(\boldsymbol{x}) \in C^{0,\alpha_3}$. There are

$$|\phi(\boldsymbol{x}) - \phi(\boldsymbol{y})| \le M_1 |\boldsymbol{x}-\boldsymbol{y}|^{\alpha_1}, \tag{3.10a}$$

$$|\boldsymbol{n}(\boldsymbol{x}) - \boldsymbol{n}(\boldsymbol{y})| \le M_2 |\boldsymbol{x}-\boldsymbol{y}|^{\alpha_2}, \tag{3.10b}$$

$$|\boldsymbol{t}(\boldsymbol{x}) - \boldsymbol{t}(\boldsymbol{y})| \le M_3 |\boldsymbol{x}-\boldsymbol{y}|^{\alpha_3}, \tag{3.10c}$$

where $0 < \alpha_i \le 1, M_i$ are all constant. Therefore, the singularity of the (2.2) and (2.4) can be removed and easily calculated by using the conventional Gaussian quadrature.

3.3. Numerical Implementation for nearly singular integrals

For boundary layer effect problems, if the interior points $\boldsymbol{y}$ are very close to the integral elements, the distance r between the interior point and the integral element tends to zero. The integrals in Eqs. (2.5) and (2.6) will behave various orders of near singularity, which can not be calculated accurately by using the conventional boundary element analysis.

For thin body problems, the domain of such structure is thin, and some boundaries will be very close to each other. Thus, the distance r between some boundary nodes and boundary integral elements probably approaches zero. This causes the integrals in discretized Eqs. (2.1) (2.4) nearly singular, and the results of the Gaussian quadrature become invalid. Therefore, the density functions cannot be calculated accurately, needless to say, to calculate the physical quantities at interior points. On the other hand, almost all the interior points are very close to the integral elements for thin body problems. Therefore, there also exist nearly singular integrals in Eqs. (2.5) and (2.6).

The above mentioned nearly singular integrals can be expressed as the following generalized integrals

$$\begin{cases} I_1 = \displaystyle\int_{\Gamma_e} \psi(\boldsymbol{x}) \ln r^2 d\Gamma, \\ I_2 = \displaystyle\int_{\Gamma_e} \psi(\boldsymbol{x}) \frac{1}{r^{2\alpha}} d\Gamma, \end{cases} \tag{3.11}$$

where $\alpha > 0, \psi(\boldsymbol{x})$ denotes a well-behaved function including the Jacobian, the shape functions and ones which arise from taking the derivative of the integral kernels. Under such a circumstance, either a very fine mesh with massive integration points or a special integration technique needs to be adopted. In the last two decades, numerous research works have been published on this subject in the BEM literature. Most of the work has been focused on the numerical approaches, such as subdivisions of the element of integration, adaptive integration schemes, exact integration methods and so on. However, most of these earlier methods are either inefficient or can not provide accurate results when the thickness of the thin structure is smaller than 1.0E-06.

In this section, a general nonlinear transformation, based on the idea of diminishing the difference of the orders of magnitude or the scale of change of operational factors, is introduced in order to remove or damp out the nearly singular properties of the Eq. (3.11).

When the collocation point $\boldsymbol{y}$ locates in the domain Ω (or Ω^c for exterior problems), then we have

$$y_1 = R_0 \cos\theta_0, \quad y_2 = R_0 \sin\theta_0, \tag{3.12}$$

where $\theta_0 = \frac{1-\eta}{2}\theta_1 + \frac{1+\eta}{2}\theta_2$ $(-1 < \eta < 1)$.

Using the procedure described in section 3.1, the distance r between the source point and the field point can be expressed as

$$r^2 = |\boldsymbol{x} - \boldsymbol{y}|^2 = 4RR_0 \left\{\sin^2\gamma + d^2\right\}, \tag{3.13}$$

where $\gamma = \beta(\xi - \eta), \beta = \frac{\theta_2 - \theta_1}{4}, d = \frac{R - R_0}{4\sqrt{RR_0}}$. The coefficients γ, β and d are determined by the coordinates of the nodes of the element and the collocation point $\boldsymbol{y}$.

Substituting r^2 in Eq. (3.13) into Eq. (3.11), then the integrals I_1 and I_2 can be divided

into two parts at point η as follows

$$\begin{cases} I_1 = \left\{ \int_{-1}^{\eta} + \int_{\eta}^{1} \right\} g(\xi) \ln(\sin^2\gamma + d^2) d\xi + \ln L^2 \int_{-1}^{1} g(\xi) d\xi, \\ I_2 = \dfrac{1}{L^{2\alpha}} \left\{ \int_{-1}^{\eta} + \int_{\eta}^{1} \right\} \dfrac{g(\xi)}{(\sin^2\gamma + d^2)^{\alpha}} d\xi, \end{cases} \tag{3.14}$$

where $L = 2\sqrt{RR_0}$ and $g(\cdot)$ is a regular function that consists of shape function, the Jacobian and a finite sum of polynomials divided by r^n .

It can be seen from Eq. (3.13) that the minimum value of r^2 equals d^2 when $\xi = \eta$. If an interior point gets close to the integral element ($R_0 \to R$), the minimum distance d^2 will trend to zero. It is obvious that the integrals in Eqs. (3.14) would present various orders of near singularity if d is very small, which can not be calculated accurately by using the standard Gaussian quadrature. The key to achieving high accuracy is to find an algorithm to calculate these integrals accurately for a small value of d.

By using some simple deduction, the integrals in Eq. (3.14) can be rewritten as follows

$$\begin{cases} I_1 = \displaystyle\int_0^{t_1} g_1(t) \ln(t^2 + d^2) dt + \int_0^{t_2} g_2(t) \ln(t^2 + d^2) dt + \ln L^2 \int_{-1}^{1} g(\xi) d\xi, \\ I_2 = \dfrac{1}{L^{2\alpha}} \left[\displaystyle\int_0^{t_1} \dfrac{g_1(t)}{(t^2 + d^2)^{\alpha}} dt + \int_0^{t_2} \dfrac{g_2(t)}{(t^2 + d^2)^{\alpha}} dt \right], \end{cases} \tag{3.15}$$

where

$$t_1 = \sin[\beta(1+\eta)], \quad t_2 = \sin[\beta(1-\eta)],$$
$$g_1(t) = \frac{1}{\beta\sqrt{1-t^2}} g\Big(\eta - \frac{1}{\beta}\arcsin t\Big), \quad g_2(t) = \frac{1}{\beta\sqrt{1-t^2}} g\Big(\eta + \frac{1}{\beta}\arcsin t\Big).$$

As long as $\theta_2 - \theta_1 \le \frac{\pi}{4}$, we have

$$|\beta(1+\eta)| = \left|\frac{\theta_0 - \theta_1}{2}\right| \le \frac{\pi}{8}, \quad |\beta(1-\eta)| = \left|\frac{\theta_0 - \theta_2}{2}\right| \le \frac{\pi}{8}, \tag{3.16}$$

according to (3.16), there should be $|t_1|$, $|t_2| = |\sin[\beta(1 \pm \eta)]| < \sin\frac{\pi}{8} \approx 0.3826834 \ll 1$. Therefore, $g_1(t)$, $g_2(t)$ are regular functions.

Introducing the following nonlinear transformation

$$t = d(e^{k_i(1+\xi)} - 1), \quad i = 1, 2, \tag{3.17}$$

where $k_1 = \ln\sqrt{1 + t_1/d}$, $k_2 = \ln\sqrt{1 + t_2/d}$. Substituting (3.17) into (3.15), then the integrals I_1 and I_2 can be rewritten as follows

$$\begin{cases} I_1 = dk_1 \ln d^2 \displaystyle\int_{-1}^{1} g_1(\xi) e^{k_1(1+\xi)} d\xi + dk_1 \int_{-1}^{1} g_1(\xi) \ln[1 + (e^{k_1(1+\xi)} - 1)^2] e^{k_1(1+\xi)} d\xi \\ \qquad + dk_2 \ln d^2 \displaystyle\int_{-1}^{1} g_2(\xi) e^{k_2(1+\xi)} d\xi + dk_2 \int_{-1}^{1} g_2(\xi) \ln[1 + (e^{k_2(1+\xi)} - 1)^2] e^{k_2(1+\xi)} d\xi, \\ \qquad + \ln L^2 \displaystyle\int_{-1}^{1} g(\xi) d\xi, \\ I_2 = \dfrac{1}{L^{2\alpha} d^{2\alpha-1}} \left\{ \displaystyle\int_{-1}^{1} \dfrac{k_1 g_1(\xi) e^{k_1(1+\xi)}}{[(e^{k_1(1+\xi)} - 1)^2 + 1]^{\alpha}} d\xi + \int_{-1}^{1} \dfrac{k_2 g_2(\xi) e^{k_2(1+\xi)}}{[(e^{k_2(1+\xi)} - 1)^2 + 1]^{\alpha}} d\xi \right\}. \end{cases} \tag{3.18}$$

It is obvious that $\ln[1 + (e^{k_1(1+\xi)} - 1)^2]$ is regular even if the value of d is very small.

By following the procedures described above, the near singularities of boundary integrals have been fully regularized. The final integral formulations over arc element are obtained as shown in Eq. (3.18), which can now be computed straightforward by using standard Gaussian quadrature.

4. Numerical Examples

In this section, both boundary layer effect and thin-body problems are given to test the proposed algorithm. The present algorithm applies the new nonlinear transformation to treat the nearly singular integrals. If the integral has no singularity, Gaussian quadrature is still kept in use.

4.1. Boundary layer effect

Example 4.1. In the first test case, which is depicted in Fig. 4.1, an infinite plate with a circular hole subjected to a uniform radial pressure $p = 10$ is considered. The radius of the circle is $r = 2$; the elastic shear modulus is $G = 807692.3N/cm^2$; the Poisson's ratio is $v = 0.3$. There are 26 uniformly arc elements divided along the boundary, and quadratic discontinuous interpolation is adopted to approximate the boundary functions.

For the interior points increasingly close to the boundary, the results of the radial and tangential stresses σ_r and σ_θ on the line $x_2 = 0$ are listed in Table 4.1 and Table 4.2, respectively. Both the CBEM and the proposed method are employed for the purpose of comparison. The convergence rates of the radial and tangential stresses σ_r and σ_θ at the point (2.0000001, 0) are shown in Fig. 4.2.

It can be seen from Table 4.1 and Table 4.2 that the results of stresses σ_r and σ_θ can be accurately calculated by using the CBEM and the present method when the computed points are not very close to the boundary ($x_1 \geq 2.1$). However, when the distance between the interior point and the boundary is equal to or less than 0.01, the results calculated by the CBEM become less satisfactory or even invalid. In contrast with the CBEM, the present method can be used

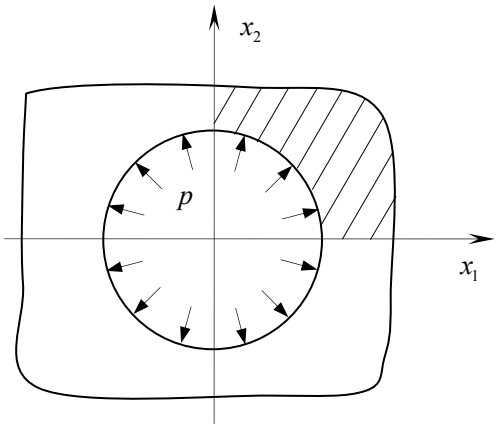

Fig. 4.1. An infinite plate with a circular hole subjected to a uniform radial pressure.

Table 4.1: Radial stresses σ_r at interior points on the line $x_2 = 0$.

x_1	Exact	CBEM	Present	Relative error (%)
2.1	-0.907029E+01	-0.906871E+01	-0.906974E+01	0.604962E-02
2.01	-0.990074E+01	0.269400E+01	-0.990064E+01	0.102934E-02
2.001	-0.999000E+01	0.715932E+01	-0.998999E+01	0.100013E-03
2.0001	-0.999900E+01	0.746507E+01	-0.999900E+01	-0.623558E-04
2.00001	-0.999990E+01	0.749544E+01	-0.999986E+01	0.382442E-03
2.000001	-0.999999E+01	0.749847E+01	-0.100000E+02	-0.408402E-03
2.0000001	-0.999999E+01	0.749878E+01	-0.999950E+01	0.491882E-02
2.00000001	-0.100000E+02	0.749881E+01	-0.100022E+02	-0.228409E-01
2.000000001	-0.100000E+02	0.749881E+01	-0.999848E+01	0.151787E-01
2.0000000001	-0.100000E+02	0.749881E+01	-0.999231E+01	0.768667E-01

Table 4.2: Tangential stresses σ_θ at interior points on the line $x_2 = 0$.

x_1	Exact	CBEM	Present	Relative error (%)
2.1	0.907029E+01	0.907065E+01	0.907076E+01	-0.514525E-02
2.01	0.990074E+01	0.747504E+01	0.990319E+01	-0.246910E-01
2.001	0.999000E+01	0.161345E+02	0.999271E+01	-0.271056E-01
2.0001	0.999900E+01	0.173662E+02	0.100017E+02	-0.274185E-01
2.00001	0.999990E+01	0.174899E+02	0.100026E+02	-0.271072E-01
2.000001	0.999999E+01	0.175023E+02	0.100027E+02	-0.270789E-01
2.0000001	0.999999E+01	0.175035E+02	0.100024E+02	-0.244594E-01
2.00000001	0.100000E+02	0.175036E+02	0.100049E+02	-0.492739E-01
2.000000001	0.100000E+02	0.175036E+02	0.100023E+02	-0.229866E-01
2.0000000001	0.100000E+02	0.175037E+02	0.999581E+01	0.418176E-01

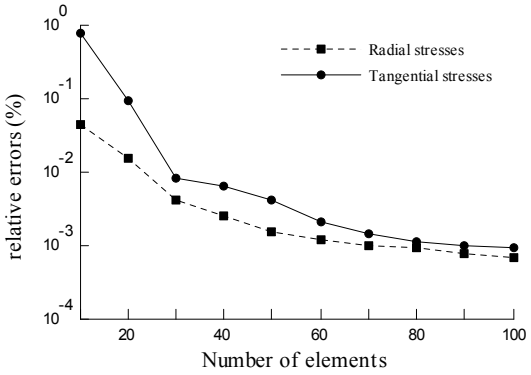

Fig. 4.2. Convergence curves of the stresses σ_r and σ_θ at the point (2.0000001, 0).

to obtain accurate results, with the largest percentage error less than 0.08%, even when the distance between the interior point and the boundary reaches 1E-10.

We can observe from Fig. 4.2 that the convergence rates of the present method are fast even when the distance between the computed point and the boundary reaches 1E-07.

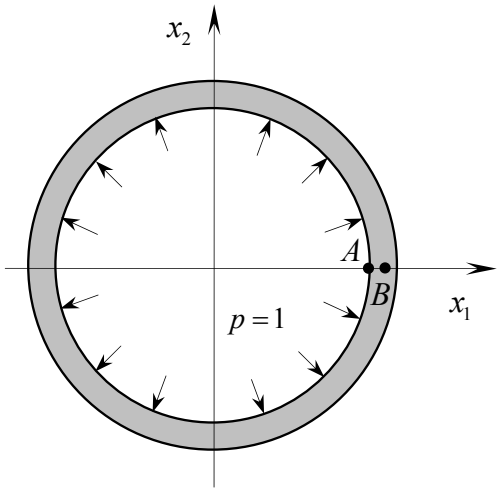

Fig. 4.3. A thin-walled cylinder subjected to uniform internal pressure.

4.2. Thin body problems

Example 4.2. As shown in Fig. 4.3, a thin-walled cylinder subjected to a uniform internal pressure $p = 1$ is considered. The outer and inner radii of the cylinder are a and b , respectively, with $a = 10$. The elastic shear modulus is $G = 807692.3N/cm^2$, and the Poisson's ratio is $v = 0.3$.

There are 50 arc elements divided along the outer and inner surfaces, and quadratic discontinuous interpolation is adopted to approximate the boundary functions. In this example, $(a - b)/a$ is defined as the thickness-to-length ratio. As a is fixed as 10, the ratio reduces as b decreases.

For different thickness-to-length ratios, the results of the unknown stresses at the boundary

Table 4.3: Radial stresses σ_r at interior points B.

x_1	Exact	CBEM	Present	Relative error (%)
1.0E-1	-0.460562E+00	-0.460387E+00	-0.460487E+00	0.162794E-01
1.0E-2	-0.496231E+00	0.958016E+01	-0.496300E+00	-0.139723E-01
1.0E-3	-0.499624E+00	-0.389405E+02	-0.499634E+00	-0.188091E-02
1.0E-4	-0.499962E+00	0.550044E+02	-0.499963E+00	-0.196719E-03
1.0E-5	-0.499996E+00	0.441747E+02	-0.499993E+00	0.528238E-03
1.0E-6	-0.499999E+00	0.433561E+02	-0.499328E+00	0.134177E+00

Table 4.4: Tangential stresses σ_θ at interior points B.

x_1	Exact	CBEM	Present	Relative error (%)
1.0E-1	0.898687E+01	0.898868E+01	0.898761E+01	-0.820917E-02
1.0E-2	0.989987E+02	0.107124E+03	0.989215E+02	0.779326E-01
1.0E-3	0.998999E+03	0.106020E+04	0.998228E+03	0.772517E-01
1.0E-4	0.999900E+04	-0.148613E+04	0.999127E+04	0.772397E-01
1.0E-5	0.999990E+05	-0.119579E+04	0.999215E+05	0.774775E-01
1.0E-6	0.999999E+06	-0.117366E+04	0.999269E+06	0.145512E+00

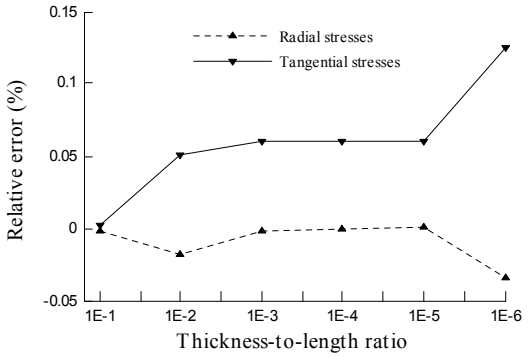

Fig. 4.4. Relative errors of σ_θ and σ_r at the boundary node A.

node $A(b,\ 0)$ are shown in Fig. 4.4. The computational results at the interior point $B((a+b)/2,\ 0)$ are listed in Table 4.3 and Table 4.4. Both the CBEM and the proposed method are employed for the purpose of comparison.

We can see from Fig. 4.4 that the calculated results of stresses at the boundary node A calculated by using the proposed method are very consistent with the exact solutions, with the largest relative error less than 0.2%, even when the thickness-to-length ratio as small as 1E-06.

Table 4.3 and Table 4.4 show that the CBEM can only be available to calculate the acceptable radial and tangential stresses at the interior point B for the thickness-to-length ratio down to 1E-01, and the results are out of true with further decrease of the thickness-to-length ratio. Nevertheless, the results obtained by using the presented schemes are excellently consistent with the analytical solutions even when the thickness-to-length ratio equals 1E-06.

Example 4.3. In this section, the method developed in this paper will be used to solve a problem of a shaft with a thin coating [19], as shown in Fig. 4.5. The shaft and coating have outer radii r_a and r_b respectively, with their centre of curvature located at the point $o(0,0)$. In this example, the coated system is loaded by a uniform pressure $p = 1$, and the shaft is considered to be rigid when compared to the coating, so the boundary conditions are $u_x = u_y = 0$ for all nodes at the shaft/coating interface. In this example, $\delta = (r_b - r_a)/r_a$ is defined as the thickness to length ratio. As r_a is held constant at 1, the ratio reduces as r_b

Table 4.5: Radial and tangential stresses at the interior point C.

δ	Radial stresses σ_r		Tangential stresses σ_θ	
	Exact	CBEM	Present	Relative error (%)
1.0E-01	-0.103232E+01	-0.103233E+01	-0.304694E+00	-0.304661E+00
1.0E-02	-0.100369E+01	-0.100361E+01	-0.255610E+00	-0.255715E+00
1.0E-03	-0.100037E+01	-0.100038E+01	-0.250562E+00	-0.250603E+00
1.0E-04	-0.100003E+01	-0.100003E+01	-0.250056E+00	-0.250172E+00
1.0E-05	-0.100000E+01	-0.100000E+01	-0.250005E+00	-0.249922E+00
1.0E-06	-0.100000E+01	-0.100000E+01	-0.250000E+00	-0.249808E+00
1.0E-07	-0.100000E+01	-0.100000E+01	-0.250000E+00	-0.249796E+00
1.0E-08	-0.100000E+01	-0.999999E+00	-0.250000E+00	-0.249795E+00
1.0E-09	-0.100000E+01	-0.100000E+01	-0.250000E+00	-0.249796E+00
1.0E-10	-0.100000E+01	-0.999998E+00	-0.250000E+00	-0.249793E+00

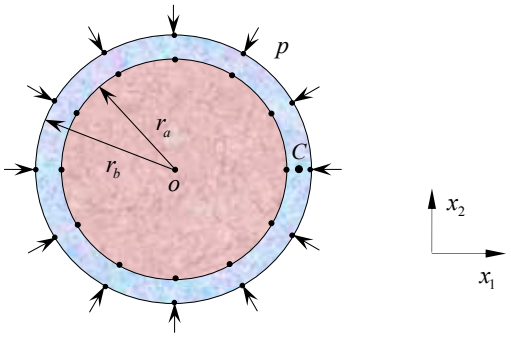

Fig. 4.5. A shaft with a thin uniform coating.

decreases.

There are totally 40 "arc elements" divided along the shaft and coating surfaces, regardless of the thickness of the structure. The elastic shear modulus is $G = 8.0 \times 10^{10}$ Pa, Poisson's ratio is $v = 0.2$.

In 1998, Luo et al. [19] have handled this coating system. However, in their work only boundary unknown radial stresses σ_r are computed. The physical quantities at interior points need further investigation.

For different thickness-to-length ratios, the results of the radial and tangential stresses at interior point $C((r_a+r_b)/2,\ 0)$ are listed in Table 4.5. For $\delta = 1.0\text{E}-9$, the results of tangential and radial stresses on the line $y = 0$ are listed in Table 4.6 and Fig. 4.6, respectively. Both the CBEM and the proposed method are employed for the purpose of comparison.

It is obvious that the results calculated by using the proposed method, shown in Table 4.5, are very consistent with the exact solutions even for the thickness to length ratio as small as 1.0E-10. We can see from Table 4.6 that the results of tangential stresses calculated by using the proposed method are very consistent with the exact solutions, with the largest relative error less than 0.09 %, even when the thickness-to-length ratio as small as 1.0E-9.

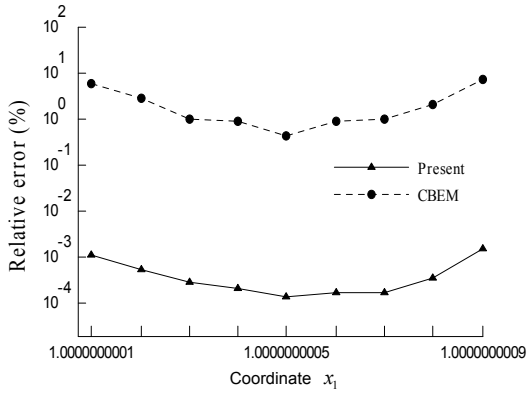

Fig. 4.6. Relative errors of Radial stresses σ_r at the interior point on the line $x_2 = 0$.

Table 4.6: Tangential stress σ_θ at the interior point on the line $x_2 = 0$.

x_1	Exact	CBEM	Present	Relative error (%)
1.0000000001	-0.25	0.205481E+01	-0.249794E+00	0.820886E-01
1.0000000002	-0.25	0.205480E+01	-0.249795E+00	0.817528E-01
1.0000000003	-0.25	0.205480E+01	-0.249796E+00	0.815571E-01
1.0000000004	-0.25	0.205480E+01	-0.249796E+00	0.814476E-01
1.0000000006	-0.25	0.205479E+01	-0.249796E+00	0.814463E-01
1.0000000007	-0.25	0.205479E+01	-0.249796E+00	0.815260E-01
1.0000000008	-0.25	0.205478E+01	-0.249795E+00	0.817607E-01
1.0000000009	-0.25	0.205478E+01	-0.249794E+00	0.820410E-01

5. Conclusions

Exact geometry representations of circular arcs are presented in this paper in order to reduce the errors caused by representing the geometries using polynomial shape functions. Both singular and nearly singular integrals are reconstructed and calculated under such geometrical representation. For boundary layer effect, the stresses at the interior points very close to the boundary can be accurately evaluated by the present method. For thin body problems with thickness-to-length ratios from 1.0E-01 to 1.0E-09, the stresses both on the boundary nodes and at interior points can be accurately calculated by using the presented strategy. Owing to the employment of exact geometrical representation, only a small number of elements need to be divided along the boundary and high accuracy can be achieved without increasing other more computational efforts.

Acknowledgement. The support of the National Natural Science Foundation of China (10571110), the Opening Fund of the State Key Laboratory of Structural Analysis for Industrial Equipment (GZ1017), and the National Natural Science Foundation of Shandong Province of China (ZR2010AZ003) are gratefully acknowledged.

References

[1] C.A. Brebbia, J.C.F, Tells and L.C. Wrobel, Boundary Element Techniques, Berlin, Heidelberg, New York, Tokyo, Springer, 1984.

[2] D.H. Yu, The Natural Boundary Integral Method and Its Applications, Science Press, Kluwer Academic Publishers, 2002.

[3] D.H. Yu, The computation of hypersingular integrals on circle and its error estimates, *Numer. Math. J. Chinese Univ*, **16**:4 (1994), 332-339.

[4] H.C. Sun, etc, Nonsingular Boundary Element Method, Dalian: Dalian University of Technology Press, 1999 (in Chinese).

[5] Y.M. Zhang, W.D. Wen and L.M. Wang, etc, A kind of new nonsingular boundary integral equations for elastic plane problems, *Acta Mech*, **36**:3 (2004), 311-321(in Chinese).

[6] D.H. Yu, The numerical computation of hypersingular integrals and its application in BEM, *Advances in Engineering Software*, **18** (1993), 103-109.

[7] C.Y. Dong, Elastoplastic crack analysis of thick-walled cylinders using the symmetric-iterative scheme of coupled BE and FE discretizations, *International Journal of Pressure Vessels and Piping*, **75**:6 (1998), 467-472.

[8] C.Y. Dong and C.J. de Pater, A boundary-domain integral equation for a coated plane problem, *Mechanics Research Communications*, **27**:6 (2000), 643-652.

[9] V. Sladek, J. Sladek and M. Tanaka, Nonsingular BEM formulations for thin-walled structures and elastostatic crack problems, *Acta Mechanica*, **99** (1993), 173-190.

[10] H.B. Chen, P. Lu P and E. Schnack, Regularized algorithms for the calculation of values on and near boundaries in 2D elastic BEM, *Engineering Analysis with Boundary Elements*, **25**:10 (2001), 851-876.

[11] Y.C. Shiah and Y.S. Shih, Regularization of nearly singular integrals in the boundary element analysis for interior anisotropic thermal field near the boundary, *Engineering Analysis with Boundary Element*, **30**:2 (2007), 219-230.

[12] M. Tanaka, T. Matsumoto and M. Nakamura, Boundary element method, Baifukan Press, Tokyo, 1991 (in Japanese).

[13] X.W. Gao, K. Yang and J. Wang, An adaptive element subdivision technique for evaluation of various 2D singular boundary integrals, *Engineering Analysis with Boundary Elements*, **32** (2008), 692-696.

[14] L. Earlin, Exact Gaussian quadrature methods for near-singular integrals in the boundary element method, *Engineering Analysis with Boundary Elements*, **9**:3 (1992), 233-245.

[15] L.F. Ma and A.M. Korsunsky, A note on the Gauss-Jacobi quadrature formulae for singular integral equations of the second kind, *International Journal of Fracture*, **126** (2004), 339-405.

[16] Z.R. Niu, C.Z. Cheng, H.L. Zhou, etc, Analytic formulations for calculating nearly singular integrals in two-dimensional BEM, *Engineering Analysis with Boundary Elements*, **31**:12 (2007), 949-964.

[17] X.S. Zhang and X.X. Zhang, Exact integrations of two-dimensional high-order discontinuous boundary element of elastostatics problems, *Engineering Analysis with Boundary Elements*, **28**:7 (2003), 725-732.

[18] Y.M. Zhang, Y. Gu and J.T. Chen, Stress analysis for multilayered coating systems using semi-analytical BEM with geometric non-linearities, *Computational Mechanics*, **47**:5 (2011), 493-504.

[19] J.F. Luo, Y.J. Liu and E.J. Berger, Analysis of two- dimensional thin structures (from micro- to nano-scales) using the boundary element method, *Computational Mechanics*, **22** (1998), 404-412.

[20] H. Ma and N. Kamiya, A general algorithm for the numerical evaluation of nearly singular boundary integrals of various orders for two- and three-dimensional elasticity, *Computational Mechanics*, **29**:4-5 (2002), 277-288.

[21] H. Ma and N. Kamiya, Distance transformation for the numerical evaluation of near singular boundary integrals with various kernels in boundary element method, *Engineering Analysis with Boundary Elements*, **26**:4 (2002), 329-339.

[22] Y.M. Zhang, Y. Gu and J.T. Chen, Analysis of 2D thin walled structures in BEM with high-order geometry elements using exact integration, *CMES: Computer Modeling in Engineering and Sciences*, **50**:1 (2009), 1-20.

[23] Y.M. Zhang, Y. Gu and J.T. Chen, Internal stress analysis for single and multilayered coating systems using the boundary element method, *Engineering Analysis with Boundary Elements*, **35** (2011), 708-717.

[24] W.C. Tang and R.T. Fenner, Analytical integration and exact geometrical representation in the two-dimensional elastostatic boundary element method, *Applied Mathematical Modelling*, **29** (2005), 1073-1099.